Progress In Electromagnetics Research, PIER 35, 141–163, 2002

ELECTROMAGNETIC SCATTERING OF A THIN CIRCULAR LOOP ENCLOSED BY A SPHERICAL CHIRAL RADOME SHELL: A METHOD OF MOMENTS ANALYSIS

L.-W. Li

Department of Electrical and Computer Engineering
National University of Singapore
10 Kent Ridge Crescent, Singapore 119260

W.-X. Zhang

State Key Laboratory of Millimeter Waves
Southeast University
2 Si-Pai-Lou, Nanjing, China 210096

Abstract—In this paper, radiation patterns of a thin circular conducting loop embedded in a two-layered spherical chiral medium but illuminated by a plane wave are obtained. The method of moments is employed in this work to formulate the current distribution along the circular loop enclosed by the spherical chiral radome shell. The dyadic Green's functions defining electromagnetic fields due to sources in both the outer and inner regions are applied. In the Galerkin's procedure for the method of moments, basis functions used in the work are sine and cosine functions which form a Fourier series. The formulation itself here is quite compact, straightforward, and easy-to-use. Effects of various geometrical and dielectric parameters of the chiral radome shell are discussed. As expected, the role of the spherical chiral radome is again realized as a polarization transformer. Associated with these parameters, waves and fields in such an electromagnetic system are characterized. It should pointed that there existed some mistakes in the literature which did not use the correct Green's functions in the method of moments procedure. This paper aims at correcting the mistake and establish a correct concept in the method of moments analysis.

1. INTRODUCTION

Chirality [1, 2] which means handedness is a property that is often encountered in the organic and biological nature. Its behavior and properties have been the researchers' subject of interest for some time. The considerable attention it receives is due to its versatility in microwave and millimeter wave applications such as waveguides, antennas, radomes, shielding, scatterers and so on and so forth. Electromagnetism in chiral and bi-isotropic media [3, 4] differs from the behavior of simpler isotropic materials in several ways. One of the aspects characterizing chiral media is the phenomenon of optical activity [5, 6].

A chiral medium is characterized by its intrinsic handedness. Its cross-coupling characteristics also makes it an interesting subject and one of the objective of this paper is to investigate how the far field pattern of the circular conducting loop [7] is affected in its presence. The constitutive relations of chiral media can be described by

$$\boldsymbol{D} = \epsilon \boldsymbol{E} + j\xi \boldsymbol{H}, \tag{1a}$$

$$\boldsymbol{H} = i\xi \boldsymbol{E} + \frac{\boldsymbol{B}}{\mu} \tag{1b}$$

where ϵ, μ and ξ are respectively, the permittivity, permeability and chirality admittance of such media.

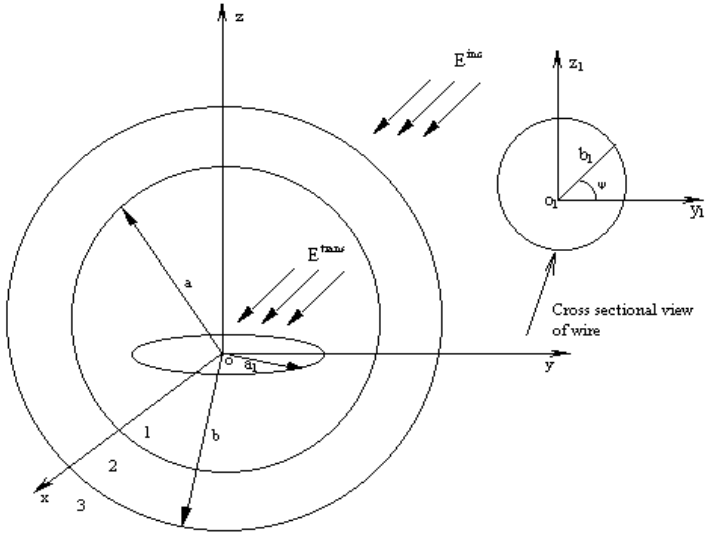

Figure 1. Geometry of a thin circular conducting loop in a two layered medium whose intermediate shell is a chiral radome.

The approach taken to find the field pattern is to obtain the current distribution flowing on it. However in the formulations of current distributions, papers [8–10] used the incident wave instead of its transmitted field. This paper attempts to investigate the effects on current distribution if the incident wave is being employed. The model used here is an electrically large conducting loop [11–18] placed in the inner most region of a two layered spherical chiral media.

2. GENERAL FORMULATIONS FOR ELECTROMAGNETIC RADIATED FIELDS

Consider the geometry in Fig. 1 where the origin of the spherical coordinates is located at the center of a two layered spherical medium with the conducting loop lying in the inner most region. The intermediate shell is considered to be a chiral radome.

The volumetric electric current of the loop is assumed to be flowing on the circumference of the wire uniformly, therefore for a delta point on its circumference, it can be expressed as

$$\delta \boldsymbol{J}_1(\boldsymbol{r}') = \frac{\delta I(\phi')\delta(r' - r_i)\delta(\theta' - \theta_i)}{2\pi r_i^2 \sin\theta_i}\widehat{\boldsymbol{\phi}} \tag{2}$$

where $I(\phi')$ identifies the current distribution that is an arbitrary function of ϕ' given by

$$\delta I(\phi') = \frac{I(\phi')\delta s}{2\pi b_1} = \frac{I(\phi')}{2\pi b_1} b_1 \partial\psi = \frac{I(\phi')}{2\pi}\partial\psi, \tag{3}$$

with $\delta s = b_1\partial\psi$, b_1 representing the cross section radius of wire, and a_1 being the radius of the loop antenna. In the method of moments, we expand the current distribution into

$$I(\phi') = \sum_{\ell=0}^{\infty} \Big[\alpha_\ell \cos(\ell\phi') + i\beta_\ell \sin(\ell\phi')\Big],$$

where α_ℓ and β_ℓ denote the unknown expansion current coefficients to be determined later on from the Galerkin's procedure.

The electromagnetic waves in the first/inner region (homogeneous medium) due to current distribution in the third/outer region (free space) are given [19]. These wave functions are

$$\begin{aligned}
\boldsymbol{V}_{\substack{e\\o}mn}(k) &= \frac{\boldsymbol{M}_{\substack{e\\o}mn}(k) + \boldsymbol{N}_{\substack{e\\o}mn}(k)}{\sqrt{2}} \\
&= \frac{1}{\sqrt{2}}\left[\mp\frac{m}{\sin\theta}P_n^m(\cos\theta)\begin{matrix}\sin\\\cos\end{matrix} m\phi\left(z_n(kr)\widehat{\boldsymbol{\theta}} + \frac{\partial[rz_n(kr)]}{kr\partial r}\widehat{\boldsymbol{\phi}}\right)\right. \\
&\quad + \frac{dP_n^m(\cos\theta)}{d\theta}\begin{matrix}\cos\\\sin\end{matrix} m\phi\widehat{\boldsymbol{\phi}}\left(\frac{\partial[rz_n(kr)]}{kr\partial r}\widehat{\boldsymbol{\theta}} - z_n(kr)\widehat{\boldsymbol{\phi}}\right) \\
&\quad \left. + \frac{n(n+1)}{kr}z_n(kr)P_n^m(\cos\theta)\begin{matrix}\cos\\\sin\end{matrix} m\phi\widehat{\boldsymbol{r}}\right], \qquad (4a) \\
\boldsymbol{W}_{\substack{e\\o}mn}(k) &= \frac{\boldsymbol{M}_{\substack{e\\o}mn}(k) - \boldsymbol{N}_{\substack{e\\o}mn}(k)}{\sqrt{2}} \\
&= \frac{1}{\sqrt{2}}\left[\pm\frac{m}{\sin\theta}P_n^m(\cos\theta)\begin{matrix}\sin\\\cos\end{matrix} m\phi\left(z_n(kr)\widehat{\boldsymbol{\theta}} - \frac{\partial[rz_n(kr)]}{kr\partial r}\widehat{\boldsymbol{\phi}}\right)\right. \\
&\quad - \frac{dP_n^m(\cos\theta)}{d\theta}\begin{matrix}\cos\\\sin\end{matrix} m\phi\widehat{\boldsymbol{\phi}}\left(\frac{\partial[rz_n(kr)]}{kr\partial r}\widehat{\boldsymbol{\theta}} + z_n(kr)\widehat{\boldsymbol{\phi}}\right) \\
&\quad \left. - \frac{n(n+1)}{kr}z_n(kr)P_n^m(\cos\theta)\begin{matrix}\cos\\\sin\end{matrix} m\phi\widehat{\boldsymbol{r}}\right], \qquad (4b)
\end{aligned}$$

where $z_n(kr)$ denotes the spherical Bessel functions of the order n and $P_n^m(\cos\theta)$ identifies the associated Legendre functions of the first kind with the order (n, m). In the region where r can be zero, we replace $z_n(kr)$ by $j_n(kr)$. And in the region where r can be infinity,

we choose $h_n^{(1)}(kr)$ instead of $z_n(kr)$. And in this case, there is usually a superscript $^{(1)}$ for this notation.

With the vector wave functions, the unbounded dyadic Green's function defining the fields of direct waves in region 1 (the inner region) due to the source excitation in region 1, $\overline{\boldsymbol{G}}_{e0}^{11}(\boldsymbol{r},\boldsymbol{r'})$, can be found. It is given for $r \gtrless r'$ as follows:

$$\overline{\boldsymbol{G}}_{e0}^{11}(\boldsymbol{r},\boldsymbol{r'}) = -\frac{\widehat{\boldsymbol{r}}\widehat{\boldsymbol{r}}}{k_1^2}\delta(\boldsymbol{r}-\boldsymbol{r'})+\frac{i}{2\pi(k_{1_+}+k_{1_-})}\sum_{n=1}^{\infty}\sum_{m=0}^{n} D_{mn} \cdot \begin{cases} k_{1_+}^2 \boldsymbol{V}_{\substack{e\\o}mn}^{(1)}(k_{1_+})\boldsymbol{V}'_{\substack{e\\o}mn}(k_{1_+})+k_{1_-}^2 \boldsymbol{W}_{\substack{e\\o}mn}^{(1)}(k_{1_-})\boldsymbol{W}'_{\substack{e\\o}mn}(k_{1_-}); \\ k_{1_+}^2 \boldsymbol{V}_{\substack{e\\o}mn}(k_{1_+})\boldsymbol{V}'^{(1)}_{\substack{e\\o}mn}(k_{1_+})+k_{1_-}^2 \boldsymbol{W}_{\substack{e\\o}mn}(k_{1_-})\boldsymbol{W}'^{(1)}_{\substack{e\\o}mn}(k_{1_-}); \end{cases} \tag{5}$$

where k_1, k_{1_+} and k_{1_-} are defined in Appendix, δ_{mn} (= 1 for $m = n$; and 0 for $m \neq n$) denotes the Kronecker symbol, and the normalization coefficient D_{mm} is given by

$$D_{mn} = (2-\delta_{m0})\frac{(2n+1)}{n(n+1)}\frac{(n-m)!}{(n+m)!}. \tag{6}$$

In a similar fashion, the unbounded dyadic Green's function defining the fields of direct waves in region 3 (the outer region) due to the source excitation in region 3, $\overline{\boldsymbol{G}}_{e0}^{33}(\boldsymbol{r},\boldsymbol{r'})$, is given for $r \gtrless r'$ as follows:

$$\overline{\boldsymbol{G}}_{e0}^{33}(\boldsymbol{r},\boldsymbol{r'}) = -\frac{\widehat{\boldsymbol{r}}\widehat{\boldsymbol{r}}}{k_3^2}\delta(\boldsymbol{r}-\boldsymbol{r'})+\frac{i}{2\pi(k_{3_+}+k_{3_-})}\sum_{n=1}^{\infty}\sum_{m=0}^{n} D_{mn} \cdot \begin{cases} k_{3_+}^2 \boldsymbol{V}_{\substack{e\\o}mn}^{(1)}(k_{3_+})\boldsymbol{V}'_{\substack{e\\o}mn}(k_{3_+})+k_{3_-}^2 \boldsymbol{W}_{\substack{e\\o}mn}^{(1)}(k_{3_-})\boldsymbol{W}'_{\substack{e\\o}mn}(k_{3_-}); \\ k_{3_+}^2 \boldsymbol{V}_{\substack{e\\o}mn}(k_{3_+})\boldsymbol{V}'^{(1)}_{\substack{e\\o}mn}(k_{3_+})+k_{3_-}^2 \boldsymbol{W}_{\substack{e\\o}mn}(k_{3_-})\boldsymbol{W}'^{(1)}_{\substack{e\\o}mn}(k_{3_-}); \end{cases} \tag{7}$$

where k_3, k_{3_+} and k_{3_-} are defined in Appendix. It should be pointed out that since both region 1 and region 3 are filled with air, so, we have

$$k_1 = k_{1_+} = k_{1_-}; \quad k_3 = k_{3_+} = k_{3_-} = k_0. \tag{8}$$

As a result, the unbounded dyadic Green's functions in regions 1 and

3 (where $s = 1, 3$) are thus reduced for $r \gtrless r'$ to

$$\overline{\boldsymbol{G}}_{e0}^{ss}(\boldsymbol{r}, \boldsymbol{r'}) = -\frac{\widehat{\boldsymbol{r}}\widehat{\boldsymbol{r}}}{k_s^2}\delta(\boldsymbol{r}-\boldsymbol{r}')+\frac{ik_s}{4\pi}\sum_{n=1}^{\infty}\sum_{m=0}^{n} D_{mn} \cdot \begin{cases} \boldsymbol{V}_{\substack{e\\o}mn}^{(1)}(k_s)\boldsymbol{V}'_{\substack{e\\o}mn}(k_s)+\boldsymbol{W}_{\substack{e\\o}mn}^{(1)}(k_s)\boldsymbol{W}'_{\substack{e\\o}mn}(k_s); \\ \boldsymbol{V}_{\substack{e\\o}mn}(k_s)\boldsymbol{V}_{\substack{e\\o}mn}^{\prime(1)}(k_s)+\boldsymbol{W}_{\substack{e\\o}mn}(k_s)\boldsymbol{W}_{\substack{e\\o}mn}^{\prime(1)}(k_s). \end{cases} \tag{9}$$

2.1. DGFs for Source in Region 1

When an electric source is located in region 1, dyadic Green's functions for a three-layered spherical chiral medium can be obtained using the method of scattering superposition and may be written as follows:

$$\overline{\boldsymbol{G}}_e^{11}(\boldsymbol{r}, \boldsymbol{r'}) = \overline{\boldsymbol{G}}_{e0}^{11}(\boldsymbol{r}, \boldsymbol{r'}) + \overline{\boldsymbol{G}}_{es}^{11}(\boldsymbol{r}, \boldsymbol{r'}), \tag{10a}$$

$$\overline{\boldsymbol{G}}_e^{21}(\boldsymbol{r}, \boldsymbol{r'}) = \overline{\boldsymbol{G}}_{es}^{21}(\boldsymbol{r}, \boldsymbol{r'}), \tag{10b}$$

$$\overline{\boldsymbol{G}}_e^{31}(\boldsymbol{r}, \boldsymbol{r'}) = \overline{\boldsymbol{G}}_{es}^{31}(\boldsymbol{r}, \boldsymbol{r'}). \tag{10c}$$

Apparently, the direct wave represented by $\overline{\boldsymbol{G}}_{e0}^{11}(\boldsymbol{r}, \boldsymbol{r'})$ exists only in region 1 while the term $\overline{\boldsymbol{G}}_{es}^{11}(\boldsymbol{r}, \boldsymbol{r'})$ in region 1 denotes the scattered waves. The other two terms, $\overline{\boldsymbol{G}}_{es}^{21}(\boldsymbol{r}, \boldsymbol{r'})$ in region 2 and $\overline{\boldsymbol{G}}_{es}^{31}(\boldsymbol{r}, \boldsymbol{r'})$ in region 3, represent transmitted wave contributions, respectively. In the formulation of the dyadic Green's functions, the multiple reflection and transmission effects have already been included in the scattering coefficients. They can be obtained from the general case found in [20] and are given as follows:

for region 1,

$$\overline{\boldsymbol{G}}_{es}^{11}(\boldsymbol{r}, \boldsymbol{r'}) = \frac{i}{4\pi k_1}\sum_{n=1}^{\infty}\sum_{m=0}^{n} D_{mn} \cdot \left\{ \left[B_1^1 \boldsymbol{V}_{\substack{e\\o}mn}(k_1)+B_2^1 \boldsymbol{W}_{\substack{e\\o}mn}(k_1)\right] \boldsymbol{V}_{\substack{e\\o}mn}^{\prime(1)}(k_1) + \left[B_3^1 \boldsymbol{V}_{\substack{e\\o}mn}(k_1)+B_4^1 \boldsymbol{W}_{\substack{e\\o}mn}(k_1)\right] \boldsymbol{W}_{\substack{e\\o}mn}^{\prime(1)}(k_1) \right\}; \tag{11a}$$

for region 2,

$$\begin{aligned}\overline{\boldsymbol{G}}_{es}^{21}(\boldsymbol{r},\boldsymbol{r'}) = \frac{i}{4\pi k_1}\sum_{n=1}^{\infty}\sum_{m=0}^{n} D_{mn} \\ \cdot\Bigg\{&\left[B_1^2\boldsymbol{V}_{\substack{e\\o}mn}(k_{2_+})+B_2^2\boldsymbol{W}_{\substack{e\\o}mn}(k_{2_-})\right]\boldsymbol{V}'^{(1)}_{\substack{e\\o}mn}(k_1) \\ &+\left[B_3^2\boldsymbol{V}_{\substack{e\\o}mn}(k_{2_+})+B_4^2\boldsymbol{W}_{\substack{e\\o}mn}(k_{2_-})\right]\boldsymbol{W}'^{(1)}_{\substack{e\\o}mn}(k_1) \\ &+\left[B_5^2\boldsymbol{V}^{(1)}_{\substack{e\\o}mn}(k_{2_+})+B_6^2\boldsymbol{W}^{(1)}_{\substack{e\\o}mn}(k_{2_-})\right]\boldsymbol{V}'^{(1)}_{\substack{e\\o}mn}(k_1) \\ &+\left[B_7^2\boldsymbol{V}^{(1)}_{\substack{e\\o}mn}(k_{2_+})+B_8^2\boldsymbol{W}^{(1)}_{\substack{e\\o}mn}(k_{2_-})\right]\boldsymbol{W}'^{(1)}_{\substack{e\\o}mn}(k_1)\Bigg\}; \quad (11b)\end{aligned}$$

and for region 3,

$$\begin{aligned}\overline{\boldsymbol{G}}_{es}^{31}(\boldsymbol{r},\boldsymbol{r'}) = \frac{i}{4\pi k_1}\sum_{n=1}^{\infty}\sum_{m=0}^{n} D_{mn} \\ \cdot\Bigg\{&\left[B_1^3\boldsymbol{V}^{(1)}_{\substack{e\\o}mn}(k_0)+B_2^3\boldsymbol{W}^{(1)}_{\substack{e\\o}mn}(k_0)\right]\boldsymbol{V}'^{(1)}_{\substack{e\\o}mn}(k_1) \\ &+\left[B_3^3\boldsymbol{V}^{(1)}_{\substack{e\\o}mn}(k_0)+B_4^3\boldsymbol{W}^{(1)}_{\substack{e\\o}mn}(k_0)\right]\boldsymbol{W}'^{(1)}_{\substack{e\\o}mn}(k_1)\Bigg\}. \quad (11c)\end{aligned}$$

2.2. DGFs for Source in Region 3

The above-given formulae of dyadic Green's functions are used to calculate the transmitted fields in region 1 due to the incident plane wave in region 3. Again using the scattering superposition method, we can obtain the total dyadic Green's functions in regions 1 to 3 as follows:

$$\overline{\boldsymbol{G}}_{e}^{13}(\boldsymbol{r},\boldsymbol{r'}) = \overline{\boldsymbol{G}}_{es}^{13}(\boldsymbol{r},\boldsymbol{r'}), \quad (12a)$$

$$\overline{\boldsymbol{G}}_{e}^{23}(\boldsymbol{r},\boldsymbol{r'}) = \overline{\boldsymbol{G}}_{es}^{23}(\boldsymbol{r},\boldsymbol{r'}), \quad (12b)$$

$$\overline{\boldsymbol{G}}_{e}^{33}(\boldsymbol{r},\boldsymbol{r'}) = \overline{\boldsymbol{G}}_{e0}^{33}(\boldsymbol{r},\boldsymbol{r'}) + \overline{\boldsymbol{G}}_{es}^{33}(\boldsymbol{r},\boldsymbol{r'}). \quad (12c)$$

Obviously, the direct wave represented by $\overline{\boldsymbol{G}}_{e0}^{33}(\boldsymbol{r},\boldsymbol{r'})$ exists only in region 3 where both source and field points are located. Certainly, there are reflected or scattered waves as well that are denoted by $\overline{\boldsymbol{G}}_{es}^{33}(\boldsymbol{r},\boldsymbol{r'})$. Out of region 3, there are only transmitted waves described by $\overline{\boldsymbol{G}}_{es}^{13}(\boldsymbol{r},\boldsymbol{r'})$ and $\overline{\boldsymbol{G}}_{es}^{23}(\boldsymbol{r},\boldsymbol{r'})$. These scattering dyadic Green's functions are given by:

for region 1,

$$\overline{\boldsymbol{G}}_{es}^{13}(\boldsymbol{r},\boldsymbol{r'}) = \frac{i}{4\pi k_0}\sum_{n=1}^{\infty}\sum_{m=0}^{n} D_{mn} \cdot\left\{\left[A_1^1\boldsymbol{V}_{\substack{e\\o}mn}(k_1)+A_2^1\boldsymbol{W}_{\substack{e\\o}mn}(k_1)\right]\boldsymbol{V}'^{(1)}_{\substack{e\\o}mn}(k_0) + \left[A_3^1\boldsymbol{V}_{\substack{e\\o}mn}(k_1)+A_4^1\boldsymbol{W}_{\substack{e\\o}mn}(k_1)\right]\boldsymbol{W}'^{(1)}_{\substack{e\\o}mn}(k_0)\right\}; \quad (13)$$

for region 2,

$$\begin{aligned}\overline{\boldsymbol{G}}_{es}^{23}(\boldsymbol{r},\boldsymbol{r'}) = \frac{i}{4\pi k_0}\sum_{n=1}^{\infty}\sum_{m=0}^{n} D_{mn} &\cdot\left\{\left[A_1^2\boldsymbol{V}_{\substack{e\\o}mn}(k_{2+})+A_2^2\boldsymbol{W}_{\substack{e\\o}mn}(k_{2-})\right]\boldsymbol{V}'^{(1)}_{\substack{e\\o}mn}(k_0)\right.\\ &+\left[A_3^2\boldsymbol{V}_{\substack{e\\o}mn}(k_{2+})+A_4^2\boldsymbol{W}_{\substack{e\\o}mn}(k_{2-})\right]\boldsymbol{W}'^{(1)}_{\substack{e\\o}mn}(k_0)\\ &+\left[A_5^2\boldsymbol{V}^{(1)}_{\substack{e\\o}mn}(k_{2+})+A_6^2\boldsymbol{W}^{(1)}_{\substack{e\\o}mn}(k_{2-})\right]\boldsymbol{W}'^{(1)}_{\substack{e\\o}mn}(k_0)\\ &\left.+\left[A_7^2\boldsymbol{V}^{(1)}_{\substack{e\\o}mn}(k_{2+})+A_8^2\boldsymbol{W}^{(1)}_{\substack{e\\o}mn}(k_{2-})\right]\boldsymbol{W}'^{(1)}_{\substack{e\\o}mn}(k_0)\right\}; \quad (14)\end{aligned}$$

and for region 3,

$$\overline{\boldsymbol{G}}_{es}^{33}(\boldsymbol{r},\boldsymbol{r'}) = \frac{i}{4\pi k_0}\sum_{n=1}^{\infty}\sum_{m=0}^{n} D_{mn} \cdot\left\{\left[A_1^3\boldsymbol{V}^{(1)}_{\substack{e\\o}mn}(k_0)+A_2^3\boldsymbol{W}^{(1)}_{\substack{e\\o}mn}(k_0)\right]\boldsymbol{V}'^{(1)}_{\substack{e\\o}mn}(k_0) + \left[A_3^3\boldsymbol{V}^{(1)}_{\substack{e\\o}mn}(k_0)+A_4^3\boldsymbol{W}^{(1)}_{\substack{e\\o}mn}(k_0)\right]\boldsymbol{W}'^{(1)}_{\substack{e\\o}mn}(k_0)\right\}; \quad (15)$$

where the unknown coefficients A_j^i (where $i = 1, 2, 3$ and $j = 1, 2, \cdots, 8$) can be solved for by manipulating matrices in Appendix. These matrix equations are obtained by applying the boundary conditions that the total tangential components of $\boldsymbol{E}$ and $\boldsymbol{H}$ must be continuous on loop's conducting surface.

3. DETERMINATION OF UNKNOWN CURRENT COEFFICIENTS

Now we determine unknown expansion coefficients of the current distribution. Before we set up the equations to be solved, we need

to analyze the total contributions of the sources to the field points. The total electric fields at an arbitrary point are given, in general, by the following relation:

$$\boldsymbol{E}^{total} = \boldsymbol{E}^{rad} + \begin{cases} \boldsymbol{E}^{trans} & \text{in region 1 or 2,} \\ \boldsymbol{E}^{ref} + \boldsymbol{E}^{inc} & \text{in region 3.} \end{cases} \tag{16}$$

Obviously, the radiated field in various regions, $\boldsymbol{E}^{rad}$, are due to the re-radiation of the conducting loop after excited by the plane wave. In the outer region 3, the total field consists of the incident plane wave, the reflected wave of the incident wave by the spherical chiral shell, and the radiated field by the loop. In region 1 or 2, the total field consists of the transmitted wave of the incident wave through the spherical chiral shell and the radiated field by the loop.

It is emphasized that in some of the previous research work, an incorrect form of the total field was sometimes used to find the current distribution in the Galerkin's procedure of method of moments. The total field was sometimes considered to consist of the incident field and the radiated field in the analysis. That approach is theoretically shown here to be incorrect although the boundary conditions were still matched later on. In this work, it is shown that the total field for matching boundary conditions on the loop's conducting surface is a superposition of the **transmitted field** and the **radiated field**.

By assuming the wire to be thin, unknown current coefficients, α_ℓ and β_ℓ, can be solved for by matching boundary condition at its center. Therefore, Eq. (16) becomes

$$E_\phi^{trans} = -E_\phi^{rad}. \tag{17}$$

To find the transmitted field $\boldsymbol{E}^{trans}$, the incident field $\boldsymbol{E}^{inc}$ obtained in [21] is expressed in an expansion form of

$$\boldsymbol{E}^{inc} = \sum_{n=1}^{\infty} \sum_{m=0}^{n} \left[P^i_{\substack{o \\ e}mn} \boldsymbol{M}_{\substack{o \\ e}mn}(k_0) + Q^i_{\substack{e \\ o}mn} \boldsymbol{N}_{\substack{e \\ o}mn}(k_0) \right], \tag{18}$$

where

$$P^i_{\substack{e \\ o}mn} = i^n D_{mn} \begin{bmatrix} \dfrac{mP_n^m(\cos\alpha)}{\sin\alpha} E_I \\ -\dfrac{\partial P_n^m(\cos\alpha)}{\partial\alpha} E_{II} \end{bmatrix}, \tag{19a}$$

$$Q^i_{\substack{e \\ o}mn} = i^n D_{mn} \begin{bmatrix} \dfrac{\partial P_n^m(\cos\alpha)}{\partial\alpha} E_I \\ -\dfrac{mP_n^m(\cos\alpha)}{\sin\alpha} E_{II} \end{bmatrix}, \tag{19b}$$

with E_I and E_{II} representing, respectively, the amplitudes of the incident electric fields of parallel and perpendicular polarizations, and α denoting the angle of incidence with respect to the $\widehat{z}$-axis.

To find the transmitted field $\boldsymbol{E}^{trans}$, there are two methodologies: one using the modal matching technique to obtain the transmitted field and the other utilizing the dyadic Green's function $\overline{\boldsymbol{G}}_{es}^{13}$. The former is direct while the latter is indirect. However, the latter is simpler than the former if the dyadic Green's functions for the medium and the geometry have already been obtained. And in fact, the dyadic Green's functions for the geometry have been obtained previously, therefore we adopt the latter approach. In this approach, it is assumed that an electric point source $\boldsymbol{J}_\infty(\boldsymbol{r}')$ is located at infinity and this source actually generates the plane wave. An alternative form of $\boldsymbol{E}^{inc}$ is shown below where $\boldsymbol{J}(\boldsymbol{r}')$ is a point source placed at infinity:

$$\begin{aligned}\boldsymbol{E}^{inc} &= i\omega\mu_0 \iiint_V \overline{\boldsymbol{G}}_{e0}(\boldsymbol{r},\boldsymbol{r}') \cdot \boldsymbol{J}_\infty(\boldsymbol{r}')dV' \\ &= -\frac{\omega\mu_0 k_0}{4\pi} \sum_{n=1}^{\infty}\sum_{m=0}^{n} D_{mn}\Bigg[\boldsymbol{M}_{\substack{e\\o}mn}(k_0) \\ &\quad \cdot \iiint_V \boldsymbol{M}'^{(1)}_{\substack{e\\o}mn}(k_0) \cdot \boldsymbol{J}_\infty(\boldsymbol{r}')dv' + \boldsymbol{N}_{\substack{e\\o}mn}(k_0) \\ &\quad \cdot \iiint_V \boldsymbol{N}'^{(1)}_{\substack{e\\o}mn}(k_0) \cdot \boldsymbol{J}_\infty(\boldsymbol{r}')dv'\Bigg]. \end{aligned} \tag{20}$$

The dyadic Green's function here is actually the free-space unbounded medium function. The incident wave can be considered as the radiated wave due to this electric source at infinity, in the absence of the chiral medium boundaries.

Obviously, (18) and (20) represent the same field, i.e., the incident field. By equating (18) to (20), the following relationships can be obtained:

$$P^i_{\substack{e\\o}mn} = -\frac{\omega\mu_0 k_0 D_{mn}}{4\pi} \iiint_V \boldsymbol{M}'^{(1)}_{\substack{e\\o}mn}(k_0) \cdot \boldsymbol{J}_\infty(\boldsymbol{r}')dV', \tag{21a}$$

$$Q^i_{\substack{e\\o}mn} = -\frac{\omega\mu_0 k_0 D_{mn}}{4\pi} \iiint_V \boldsymbol{N}'^{(1)}_{\substack{e\\o}mn}(k_0) \cdot \boldsymbol{J}_\infty(\boldsymbol{r}')dV'. \tag{21b}$$

These relations can thus be employed to shorten our procedure of determining the transmitted fields inside the empty region 1 enclosed by the chiral shell. By employing the coefficients in (21), $\boldsymbol{E}^{trans}$ can be found as follows:

$$\boldsymbol{E}^{trans} = i\omega\mu_0 \iiint_V \overline{\boldsymbol{G}}_e^{13}(\boldsymbol{r},\boldsymbol{r}') \cdot \boldsymbol{J}_\infty(\boldsymbol{r}')dV'$$

$$= -\frac{\omega\mu_1}{4\pi k_1^3}\sum_{n=1}^{\infty}\sum_{m=0}^{n} D_{mn}\left\{\left[\left(A_1^1+A_2^1\right)P^i_{e_{omn}}\right.\right.$$
$$+\left(A_3^1+A_4^1\right)Q^i_{e_{omn}}\Big]\boldsymbol{M}_{e_{omn}}(k_1)+\Big[\left(A_1^1-A_2^1\right)P^i_{e_{omn}}$$
$$\left.+\left(A_3^1-A_4^1\right)Q^i_{e_{omn}}\Big]\boldsymbol{N}_{e_{omn}}(k_1)\right\}, \tag{22}$$

where the coefficients, A_1^1 to A_4^1, are obtainable from matrix manipulations in Appendix.

Physically, $\boldsymbol{E}^{rad}$ in (17) arises from superposition of $\delta\boldsymbol{E}^{rad}$ which is due to the contribution of line filament currents flowing along the circumference of the wire. Theoretically, $\delta\boldsymbol{E}^{rad}$ can be expressed as

$$\begin{aligned}\delta\boldsymbol{E}^{rad} &= i\omega\mu_0\iiint_V \overline{\boldsymbol{G}}_e^{11}(\boldsymbol{r},\boldsymbol{r'})\cdot\boldsymbol{J}_1(\boldsymbol{r'})dV'\\ &= i\omega\mu_0\iiint_V\left\{\overline{\boldsymbol{G}}_{e0}^{11}(\boldsymbol{r},\boldsymbol{r'})+\overline{\boldsymbol{G}}_{es}^{11}(\boldsymbol{r},\boldsymbol{r'})\right\}\cdot\boldsymbol{J}_1(\boldsymbol{r'})dV'\\ &= \delta\boldsymbol{E}_{0i}^{rad}+\delta\boldsymbol{E}_{0ii}^{rad}+\delta\boldsymbol{E}_s^{rad},\end{aligned} \tag{23}$$

where $\delta\boldsymbol{E}_{0i}^{rad}$ accounts for the contribution due to $\overline{\boldsymbol{G}}_{e0}^{11}(\boldsymbol{r},\boldsymbol{r'})$ for $r<r'$, while $\delta\boldsymbol{E}_{0ii}^{rad}$ due to $\overline{\boldsymbol{G}}_{e0}^{11}(\boldsymbol{r},\boldsymbol{r'})$ for $r>r'$ and $\delta\boldsymbol{E}_s^{rad}$ due to $\overline{\boldsymbol{G}}_{es}^{11}(\boldsymbol{r},\boldsymbol{r'})$ for both $r>r'$ and $r<r'$. As Eq. (23) is a function of ψ, the total radiated field $\boldsymbol{E}^{rad}$ can thus be found by integrating the elementary contribution with respect to ψ, that is,

$$\boldsymbol{E}^{rad}=i\omega\mu_0\iiint_V\left[\overline{\boldsymbol{G}}_{e0}(\boldsymbol{r},\boldsymbol{r'})+\overline{\boldsymbol{G}}_{es}^{11}(\boldsymbol{r},\boldsymbol{r'})\right]\cdot\boldsymbol{J}_1(\boldsymbol{r'})dV'd\psi. \tag{24}$$

Using the Galerkin's method together with (17), (20), (22), and (23), the unknown coefficients, α_ℓ and β_ℓ, are found.

4. ELECTROMAGNETIC FIELDS IN THE FAR ZONES

The electric far-zone field can be obtained using the dyadic Green's function as expressed in (11c). For far field, the following approximation on $\boldsymbol{J}(\boldsymbol{r'})$ can be made:

$$\begin{aligned}\boldsymbol{J}(\boldsymbol{r'}) &= \frac{\delta I(\phi')\delta(r'-r_i)\delta(\theta'-\theta_i)}{2\pi r_i^2\sin\theta_i}\widehat{\boldsymbol{\phi}}\\ &\approx \frac{\delta I(\phi')\delta(r'-a_1)\delta(\theta'-\pi/2)}{2\pi a_1^2}\widehat{\boldsymbol{\phi}},\end{aligned} \tag{25}$$

where a_1 is the radius of the loop antenna. The radiated field, $\boldsymbol{E}^{rad}$, is therefore given by

$$\boldsymbol{E}^{rad} = i\omega\mu_0 \iiint_V \overline{\boldsymbol{G}}_e^{31}(\boldsymbol{r}, \boldsymbol{r'}) \cdot \widehat{\phi} \frac{d\psi}{2\pi} \frac{I(\phi')\delta(r' - a_1)\delta(\theta' - \pi/2)}{2\pi a_1^2} dV' \quad (26)$$

where

$$dV' = r_i^2 \sin\theta_i dr_i d\theta_i d\phi. \quad (27)$$

5. NUMERICAL RESULTS

After we establish the theory shown as above, numerical computations are made to gain insight into physical significance of the problem. Discussion is divided into two parts, one on the correct application of moment method and the other one on effects of chiral parameter. Two quantities are actually considered in the numerical computations, namely, the current distribution on the circular conducting loop and the radiation patterns of the loop.

5.1. Use of Incident Field

As mentioned earlier, the total field used in the method of moments procedure is assumed in some of the existing work to be the superposition of the incident field (from infinity) and the radiated field (from the conducting loop). It is shown in the present work that the total field should be the sum of the transmitted field (from infinity to the region where the loop is located) and the radiated field (from the loop). People may argue about that the solution generated in the scattering system should be the same according to the uniqueness theorem regardless of if the incident wave or its generated transmitted wave is used. Subsequently, it is shown that the two sets of the results are not the same and so the use of the direct incident wave is incorrect.

Figs. 2–4 show the variations to current distributions when $\boldsymbol{E}^{trans}$ and $\boldsymbol{E}^{inc}$ are used. The parameters used here to obtain the results are as follows: $\mu_2 = \mu_0$, $\mu_1 = 1.1\mu_0$, $\epsilon_1 = 2.1\epsilon_0$, $\epsilon_2 = 2.5\epsilon_0$, $\xi_2 = \xi = 2 \times 10^{-3}$, $f = 10$ GHz, $E_I = 1$, $E_{II} = 1$ and $\alpha = \frac{\pi}{4}$. The radius of the inner most sphere, a, is λ while the radius of the outer sphere, b, has a value of 1.5λ. The relationship between the loop and wire cross section radii is $2\ln(2\pi a/b) = 10$. Convergence is checked and the infinity sign in (24) is replaced by 300 which varies with dimension of the scattering system and may be reduced if the chiral shell is electrically smaller.

It is seen from Figs. 2–4 that when the loop dimension is small, the current flowing along the conducting loop does not vary so dramatically

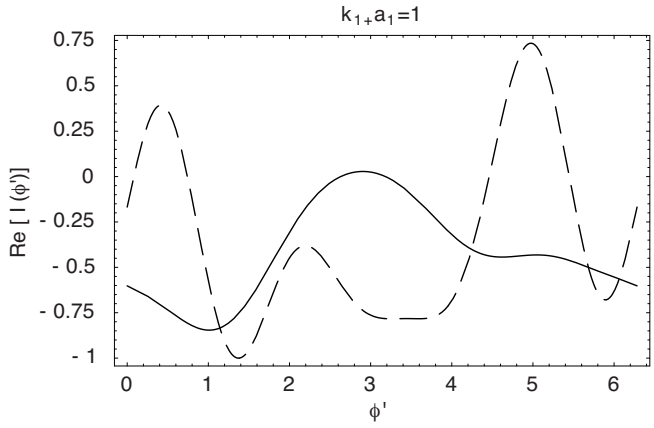

(a) Real part

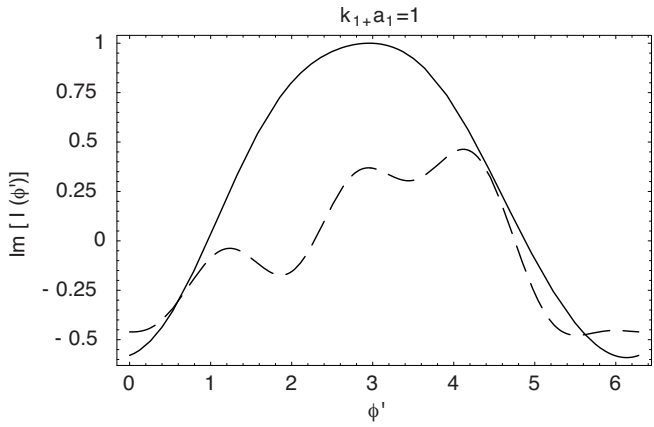

(b) Imaginary part

Figure 2. Current distributions for $k_{1+}a_1 = k_{1-}a_1 = k_0a_1 = 1$. Solid and dash curves represent the results from utilizations of $\boldsymbol{E}^{trans}$ and $\boldsymbol{E}^{inc}$, respectively.

(as in Fig. 2). However, the current becomes dramatically oscillating when the loop dimension is large (as in Fig. 4). So more cosine terms are needed to model the current distributions when the loop size increases.

Also, it is seen from Figs. 2–4 that the use of $\boldsymbol{E}^{trans}$ and $\boldsymbol{E}^{inc}$ in the method of moments procedure gives quite different results of current distributions. The real parts of the current are always large regardless of the loop dimension while the imaginary part differs considerably as

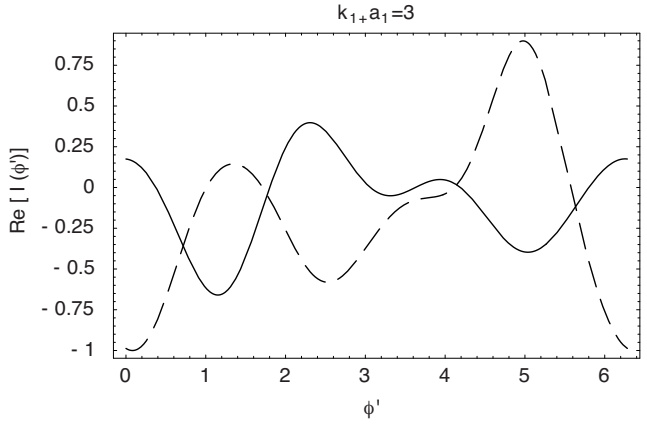

(a) Real part

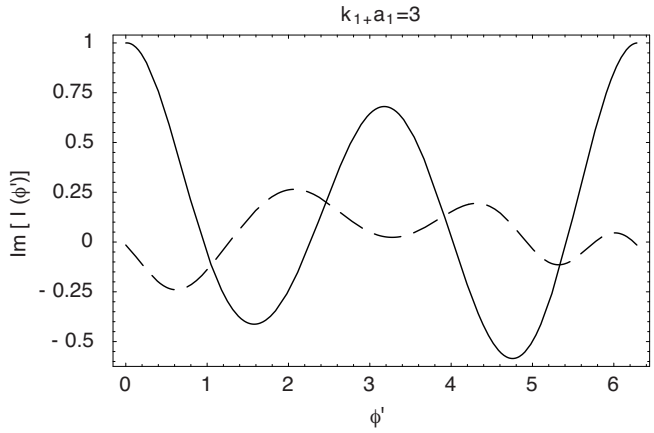

(b) Imaginary part

Figure 3. Current distributions for $k_{1+}a_1 = k_{1-}a_1 = k_0a_1 = 3$. Solid and dash curves represent the results from utilizations of $\boldsymbol{E}^{trans}$ and $\boldsymbol{E}^{inc}$, respectively.

the size is small and becomes closer as the size is large. Therefore, a proper fields should be used in the analysis. This is very important especially when you need to calculate the input impedance which requires the information of the near-field and current distribution.

For some problems, even the current distribution or input impedance of the system is different but the far-zone field does not vary much, when different methods are employed. For the current problem here, it is found that field patterns due to the above current

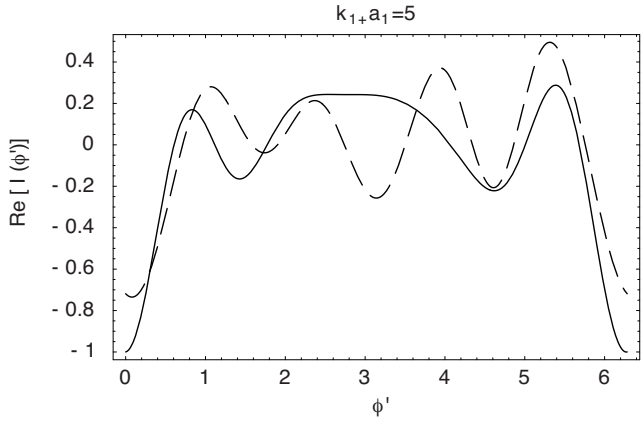

(a) Real part

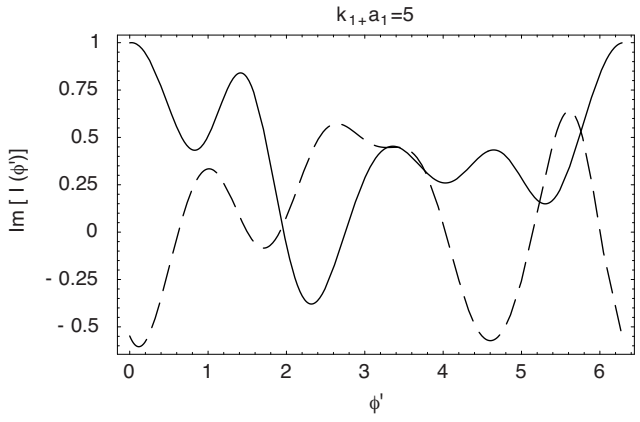

(b) Imaginary part

Figure 4. Current distributions for $k_{1+}a_1 = k_{1-}a_1 = k_0a_1 = 5$. Solid and dash curves represent the results from utilizations of $\boldsymbol{E}^{trans}$ and $\boldsymbol{E}^{inc}$, respectively.

distributions vary a lot when the expressions $\boldsymbol{E}^{trans}$ and $\boldsymbol{E}^{inc}$ in the method of moments procedure are used, shown in Figs. 5–7.

Three planes here are considered, namely, x-z plane, y-z plane and x-y plane. It is seen from the comparison among these figures that more changes are observed in the y-z plane when the loop dimension is small and changes become dramatical in all the planes when the loop dimension is large.

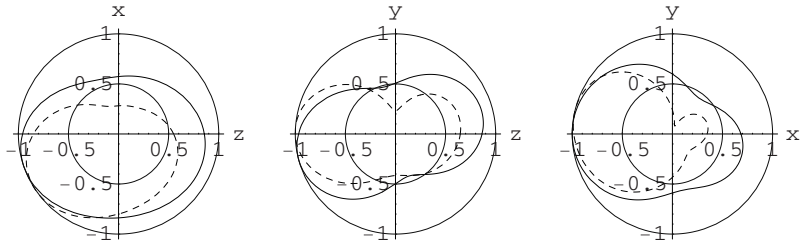

Figure 5. Field patterns for $k_0 a_1 = 1$. Solid and dash curves represent the results from utilizations of $\boldsymbol{E}^{trans}$ and $\boldsymbol{E}^{inc}$, respectively.

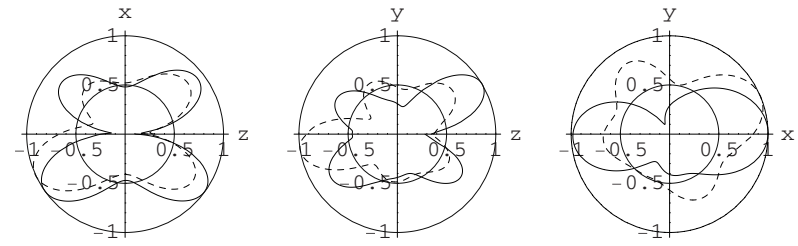

Figure 6. Field patterns for $k_0 a_1 = 3$. Solid and dash curves represent the results from utilizations of $\boldsymbol{E}^{trans}$ and $\boldsymbol{E}^{inc}$, respectively.

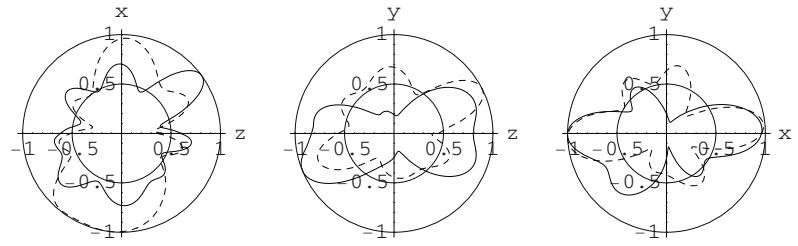

Figure 7. Field patterns for $k_0 a_1 = 5$. Solid and dash curves represent the results from utilizations of $\boldsymbol{E}^{trans}$ and $\boldsymbol{E}^{inc}$, respectively.

5.2. Effects of Chiral Parameters

In order to investigate effects of ξ on the current distributions and their resultant field patterns, we varied the value of chiral parameter ξ and assumed the inner region to be free space. The dielectric parameters used are as follows: $\mu 1 = \mu_0$, $\epsilon_1 = \epsilon_0$, $f = 10$ GHz, $E_I = 1$, $E_{II} = 1$ and $\alpha = \frac{\pi}{4}$ with ξ (actually ξ_2) as the variable. Other dielectric and geometrical parameters are the same as those in Figs. 2–4. Fig. 8 plots

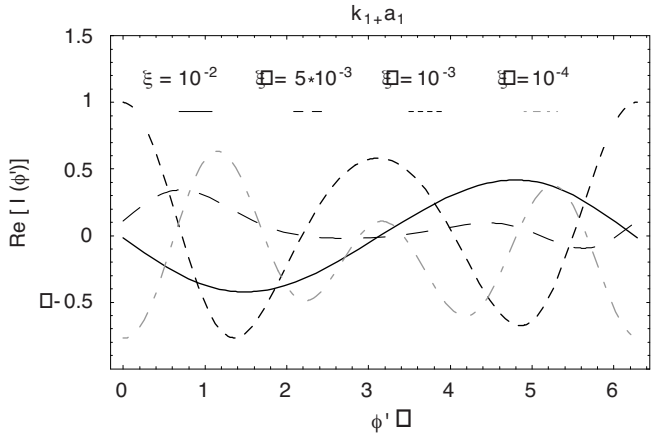

(a) Real part

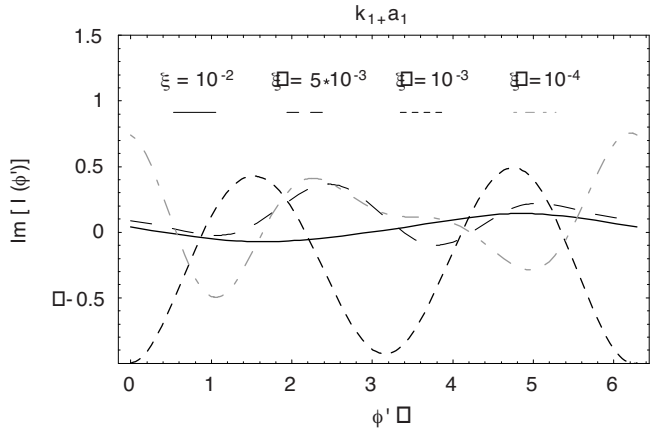

(b) Imaginary part

Figure 8. Current distributions against ξ.

the real and imaginary parts of the current distributions against ξ as the varying parameter, demonstrating the diverse property of chiral material.

The real and imaginary parts of current distributions do not vary proportionally with changes in the parameter, ξ. It is known from [14, 7] that as the loop size increases, more terms of the cosine and sine series are needed so as to achieve the accuracy and/or convergence. For the case when the conducting loop is placed in a one-layered chiral medium, Fig. 8 shows that the chiral parameter can, to a certain extent,

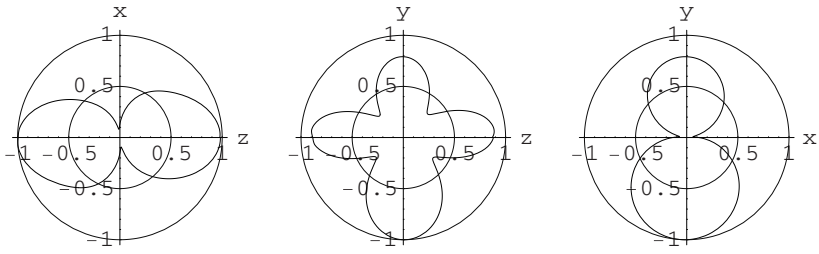

Figure 9. Field patterns for $\xi = 10^{-3}$ and $k_0 a_1 = 3$.

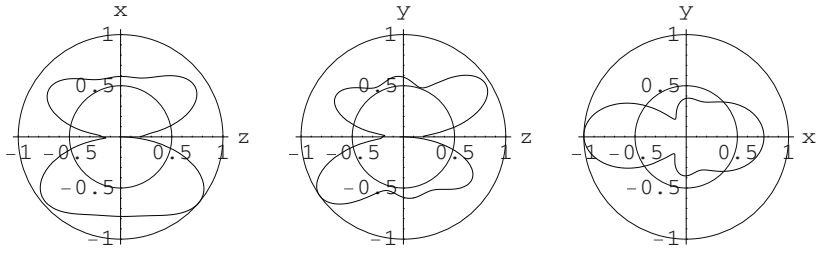

Figure 10. Field patterns for $\xi = 3 \times 10^{-3}$ and $k_0 a_1 = 3$.

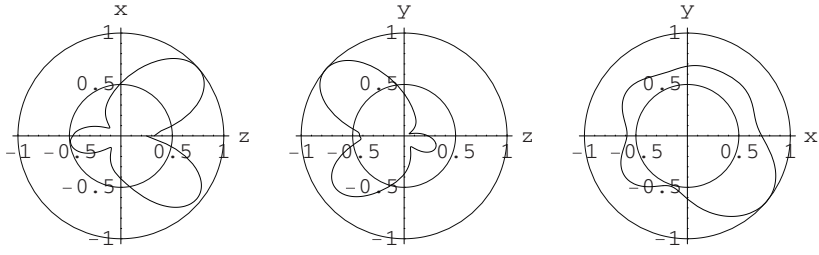

Figure 11. Field patterns for $\xi = 5 \times 10^{-3}$ and $k_0 a_1 = 3$.

affect the number of terms needed to model the current distributions. The fact that chiral media has provided us with an additional freedom to vary the electromagnetic fields is indisputable.

The field patterns for various value of ξ are shown subsequently in Figs. 9–11. It is shown that the field patterns change dramatically with the chiral parameter ξ. This provides another way of achieving desired antenna patterns in the antenna designs and antenna applications.

6. CONCLUSION

This paper presents an approach of analyzing far-field radiation patterns of a conducting loop embedded in chiral media that is illuminated by a plane wave. The dyadic Green's functions for the layered chiral media and the Galerkin's procedure of method of moments are both employed in the characterization. In the Galerkin's procedure, the basis functions used are the Fourier series. The analysis illustrates the cross-polarization properties of chiral materials. For a conducting loop radiating in free space, the number of cosine and sine functions needed for the current distributions are determined by the loop size. For the same loop embedded in chiral media, however, the number of terms required can be controlled by both the loop dimension and the chiral parameter ξ. So, the convergence number may not very large provided that an appropriate chiral parameter is chosen. Another point made in this work is that for correctly characterizing an antenna embedded in a (chiral or achrial) material, the excitation field should be the transmitted wave due to the multiple interactions of the layered structure instead of the incident field itself at infinity. It is demonstrated in this paper that the misuse of an incident wave at infinity in the media for the transmitted wave can result in a large error in the antenna current distribution (or its associated input impedance) as well as in the far-field patterns. Finally, it is realized in the paper that the use of chiral material for the radiating system provides another way of achieving desired antenna patterns in the antenna designs and antenna applications.

ACKNOWLEDGMENT

This work has been supported in part by Visiting Scholar Foundation of Key Lab In University through State Key Laboratory of Millimeter Waves at Southeast University, China and by a research grant of National Science and Technology Board (NSTB), Singapore through the National University of Singapore. The first author is grateful to Mr. Suan-Yee Tan for generating some of the plots with the given theory and an algorithm.

APPENDIX A. DETERMINATION OF PARAMETERS

$$[\boldsymbol{D}]\cdot\begin{pmatrix}\boldsymbol{B}_1^1\\ \boldsymbol{B}_2^1\\ \boldsymbol{B}_5^2\\ \boldsymbol{B}_6^2\\ \boldsymbol{B}_1^2\\ \boldsymbol{B}_2^2\\ \boldsymbol{B}_1^3\\ \boldsymbol{B}_2^3\end{pmatrix}=\begin{pmatrix}-k_{1_+}^2 h_{1_+}^b\\ -k_{1_+}^2\partial h_{1_+}^b\\ k_{1_+}^2 h_{1_+}^b\\ k_{1_+}^2\partial h_{1_+}^b\\ 0\\ 0\\ 0\\ 0\end{pmatrix}, \tag{A1a}$$

$$[\boldsymbol{D}]\cdot\begin{pmatrix}\boldsymbol{B}_3^1\\ \boldsymbol{B}_4^1\\ \boldsymbol{B}_7^2\\ \boldsymbol{B}_8^2\\ \boldsymbol{B}_3^2\\ \boldsymbol{B}_4^2\\ \boldsymbol{B}_3^3\\ \boldsymbol{B}_3^3\end{pmatrix}=\begin{pmatrix}-k_{1_-}^2 h_{1_-}^b\\ k_{1_-}^2\partial h_{1_-}^b\\ -k_{1_-}^2 h_{1_-}^b\\ k_{1_-}^2\partial h_{1_-}^b\\ 0\\ 0\\ 0\\ 0\end{pmatrix}, \tag{A1b}$$

$$[\boldsymbol{D}]\cdot\begin{pmatrix}\boldsymbol{A}_1^1\\ \boldsymbol{A}_2^1\\ \boldsymbol{A}_5^2\\ \boldsymbol{A}_6^2\\ \boldsymbol{A}_1^2\\ \boldsymbol{A}_2^2\\ \boldsymbol{A}_1^3\\ \boldsymbol{A}_2^3\end{pmatrix}=\begin{pmatrix}0\\ 0\\ 0\\ 0\\ k_0^2 j_0^b\\ k_0^2\partial j_0^b\\ l_2 k_0^2 j_0^b\\ l_2 k_0 2\partial j_0^b\end{pmatrix}, \tag{A1c}$$

$$[\boldsymbol{D}]\cdot\begin{pmatrix}\boldsymbol{A}_3^1\\ \boldsymbol{A}_4^1\\ \boldsymbol{A}_7^2\\ \boldsymbol{A}_8^2\\ \boldsymbol{A}_3^2\\ \boldsymbol{A}_4^2\\ \boldsymbol{A}_3^3\\ \boldsymbol{A}_3^3\end{pmatrix}=\begin{pmatrix}0\\ 0\\ 0\\ 0\\ k_0^2 j_0^b\\ -k_0^2\partial j_0^b\\ -l_2 k_0^2 j_0^b\\ l_2 k_0 2\partial j_0^b\end{pmatrix}; \tag{A1d}$$

where

$$l_1=\frac{\mu_1\sqrt{k_2^2+\omega^2\mu_2^2\xi_2^2}}{\mu_2\sqrt{k_1^2+\omega^2\mu_1^2\xi_1^2}}, \tag{A2a}$$

$$l_2 = \frac{\mu_2 k_0}{\mu_0 \sqrt{k_2^2 + \omega^2 \mu_2^2 \xi_2^2}}; \tag{A2b}$$

with

$$k_j = \omega\sqrt{\mu_j \epsilon_j}, \tag{A3a}$$

$$k_{j\pm} = \pm\,\omega\mu_j\xi_j + \sqrt{k_j^2 + \omega^2\mu_j^2\xi_j^2}, \tag{A3b}$$

$$j_{j\pm}^{r_i} = j_n(k_{j\pm} r_i), \tag{A3c}$$

$$\partial j_{j\pm}^{r_i} = \frac{1}{k_{j\pm r_i}} \left[\frac{d[r j_n(k_{j\pm} r)]}{dr}\right]_{r=r_i}, \tag{A3d}$$

$$h_{j\pm}^{r_i} = h_n^{(1)}(k_{j\pm} r_i)$$

$$\partial h_{j\pm}^{r_i} = \frac{1}{k_{j\pm r_i}} \left[\frac{d[r h_n^{(i)}(k_{j\pm} r)]}{dr}\right]_{r=r_i}; \tag{A3e}$$

$$[\boldsymbol{D}] = \begin{bmatrix} j_{1_+}^a & j_{1_-}^a & -h_{2_+}^a & -h_{2_-}^a & -j_{2_+}^a & -j_{2_-}^a & 0 & 0 \\ \partial j_{1_+}^a & -\partial j_{1_-}^a & -\partial h_{2_+}^a & \partial h_{2_-}^a & -\partial j_{2_+}^a & \partial j_{2_-}^a & 0 & 0 \\ -j_{1_+}^a & j_{1_-}^a & l_1 h_{2_+}^a & -l_1 h_{2_-}^a & l_1 j_{2_+}^a & -l_1 j_{2_-}^a & 0 & 0 \\ -\partial j_{1_+}^a & -\partial j_{1_-}^a & l_1 \partial h_{2_+}^a & l_1 \partial h_{2_-}^a & l_1 \partial j_{2_+}^a & l_1 \partial j_{2_-}^a & 0 & 0 \\ 0 & 0 & h_{2_+}^b & h_{2_-}^b & j_{2_+}^b & j_{2_-}^b & -h_0^b & -h_0^b \\ 0 & 0 & \partial h_{2_+}^b & -\partial h_{2_-}^b & \partial j_{2_+}^b & -\partial j_{2_-}^b & -\partial h_0^b & \partial h_0^b \\ 0 & 0 & h_{2_+}^b & -h_{2_-}^b & j_{2_+}^b & -j_{2_-}^b & -l_2 h_0^b & l_2 h_0^b \\ 0 & 0 & \partial h_{2_+}^b & \partial h_{2_-}^b & \partial j_{2_+}^b & \partial j_{2_-}^b & -l_2 \partial h_0^b & -l_2 \partial h_0^b \end{bmatrix}. \tag{A4}$$

REFERENCES

1. Lakhtakia, A., V. K. Varadan, and V. V. Varadan, *Time-Harmonic Electromagnetic Fields in Chiral Media*, Springer, Berlin, 1989.
2. Lindell, I. V. and A. H. Sihvola, "Plane wave reflection from uniaxial chiral interface and its application to polarization transformation," *IEEE Trans. Antennas Propagat.,* Vol. AP-43, No. 12, 1397–1404, 1995.
3. Kong, J. A., *Electromagnetic Wave Theory*, John Wiley & Sons, New York, 3rd edition, 1990.
4. Dmitriev, V. A., "Constitutive tensors and general properties of complex bianisotropic media described by continuous groups of

symmetry," *Electronic Letters*, Vol. 34, No. 6, 532–534, March 1998.

5. Lindell, I. V., A. H. Sihvola, S. A. Tretyakov, and A. J. Viitanen, *Electromagnetic Waves in Chiral and Bi-Isotropic Media*, Artech House, Boston, 1994.
6. Lindell, I. V. and A. J. Viitanen, "Duality transformations for general bi-isotropic (nonreciprocal chiral) media," *IEEE Trans. Antennas Propagat.,* Vol. AP-40, No. 1, 91–95, Jan. 1992.
7. Balanis, C. A., *Advanced Engineering Electromagnetics,* John Wiley & Sons, New York, 1989.
8. Tsai, M.-J., F. De Flaviis, O. Fordham, and N. G. Alexopoulos, "Modeling planar arbitrary shaped microstrip elements in multilayered media," *IEEE Trans. Microwave Theory Tech.,* Vol. MTT-45, No. 3, 330–337, Mar. 1997.
9. Raut, S. and A. Sebak, "An efficient method for the design and analysis of microstrip circuits and antennas," *1997 Conference on Communications, Power and Computing* WESCANEX'97*, Winnipeg, MB*, 233–237, May 22–23, 1997.
10. Robinson, B., T. Vlasits, E. Korolkiewicz, and C. Creasy, "Moment method analysis of an aperture coupled microstrip antenna with multilayer superstrate," *The* 3^{rd} *International Conference on Computation in Electromagnetics,* 10–12, IEE Press, UK, 1996.
11. Werner, D. H., "An exact integration procedure for vector potentials of thin circular loop antennas," *IEEE Trans. Antennas Propagat.,* Vol. AP-44, No. 2, 157–165, 1996.
12. Overfelt, P. L., "Near fields of the constant current thin circular loop antenna of arbitrary radius," *IEEE Trans. Antennas Propagat.,* Vol. AP-44, No. 2, 166–171, Feb. 1996.
13. Li, L.-W., M.-S. Leong, P.-S. Kooi, and T.-S. Yeo, "Exact solutions of electromagnetic fields in both near and far zones radiated by thin circular loop antennas: A general representation," *IEEE Trans. Antennas Propagt.,* Vol. 45, No. 12, 1741–1748, December 1997.
14. Li, L.-W., C.-P. Lim, and M.-S. Leong, "Method of moments analysis of electrically large circular-loop antennas: Non-uniform currents," *IEE Proceedings on Microwave, Antennas and Propagation,* Vol. 146, No. 6, 416–420, November–December 1999.
15. Kanda, M., "An electromagnetic near-field sensor for simultaneous electric and magnetic-field measurements," *IEEE Trans. Electromagn. Compat.,* Vol. EMC-26, No. 3, 102–110, Aug. 1984.

16. Wu, T. T., "Theory of the thin circular loop antenna," *J. Math. Phys.,* Vol. 3, 1301–1304, Dec. 1962.
17. Sarkar, T. K., "A study of the various methods for computing electromagnetic field utilizing thin wire integral equations," *Radio Sci.,* Vol. 18, 29–38, 1983.
18. Blackburn, R. F. and D. R. Wilton, "Analysis and synthesis of an impedance-loaded loop antenna using the singularity expansion method," *IEEE Trans. Antennas Propagat.,* Vol. AP-26, No. 1, 136–140, Jan. 1978.
19. Engheta, N. and M. W. Kowarz, "Antenna radiation in the presence of a chiral sphere," *J. Appl. Phys.,* Vol. 67, No. 2, 639–647, 1990.
20. Li, L.-W., P.-S. Kooi, M.-S. Leong, and T.-S. Yeo, "A general expression of dyadic Green's function in radially multilayered chiral media," *IEEE Trans. Antennas Propagat.,* Vol. 43, No. 3, 232–238, March 1995.
21. Morrison, J. A. and M. J. Cross, "Scattering of a plane electromagnetic wave by axisymmetric raindrops," *Bell Syst. Tech. J.,* Vol. 53, 955–1019, 1974.